Nanoscale

Synthesis of air-stable two-dimensional nanoplatelets of Ruddlesden-Popper organic-inorganic hybrid perovskites

Journal:	*Nanoscale*
Manuscript ID	NR-COM-12-2019-010543.R1
Article Type:	Paper
Date Submitted by the Author:	13-Mar-2020
Complete List of Authors:	Cherusseri, Jayesh; Univeristy of Central Florida, NanoScience Technology Center Varma, Sreekanth; Univeristy of Central Florida, NanoScience Technology Center; Department of Physics Pradhan, Basudev; University of Central Florida, NanoScience Technology Center Li, Jinxin; University of Central Florida, CREOL, College of Optics and Photonics Kumar , Jitesh ; University of Central Florida Barrios , Elizabeth ; University of Central Florida Amin, Muhammad ; University of Central Florida Towers, Andrew; University of Central Florida Gesquiere, Andre; University of Central Florida, NanoScience Technology Center, Department of Chemistry and CREOL Thomas, Jayan; University of Central Florida, NanoScience Technology Center; CREOL, College of Optics and Photonics

Synthesis of air-stable two-dimensional nanoplatelets of Ruddlesden-Popper organic-inorganic hybrid perovskites

Jayesh Cherusseri[1+], Sreekanth J Varma[1+], Basudev Pradhan[1], Jinxin Li[1,2], Jitesh Kumar[1,2], Elizabeth Barrios[1,4], Mohammed Zain Amin[1], Andrew Towers[1,3], Andre Gesquiere[1,2,3], Jayan Thomas[1,2,4*]

[1]NanoScience Technology Center, University of Central Florida, Orlando, Florida 32826, USA
[2]CREOL, The College of Optics and Photonics, University of Central Florida, Orlando, Florida 32816, USA
[3]Department of Chemistry, University of Central Florida, Orlando, Florida 32816, USA
[4]Department of Materials Science and Engineering, University of Central Florida, Orlando, Florida 32816, USA

[+]These authors contributed to this work equally

*Corresponding Author E-mail: Jayan.Thomas@ucf.edu

Abstract

We present a simple and facile method to synthesize nanoplatelets of 2D Ruddlesden–Popper (RP) perovskite of the type $(CH_3(CH_2)_3NH_3)_2(CH_3NH_3)Pb_2I_7$ where n = 2. The 2D RP nanoplatelets are synthesized from the bulk 2D RP crystals via. a reflux pre-treatment mediated-ultrasonication method. The as-synthesized 2D RP nanoplatelets are highly air-stable even after two months of storage under ambient atmosphere. The bulk 2D RP crystals and 2D RP nanoplatelets are characterized using X-ray diffraction, scanning electron microscopy, transmission electron microscopy, Kelvin probe force microscopy, UV-visible spectroscopy, X-ray photoelectron spectroscopy (XPS), photoluminescence, time correlated single photon counting measurement, etc. A significant blue shift in the ultraviolet-visible absorption spectrum, high photoluminescence in the UV region, and the modified work function of the nanoplatelets indicate a strong quantum confinement effect. The quantum confinement in the nanoplatelets is further confirmed using XPS. A photodetector fabricated using these 2D RP nanoplatelets exhibits a high photodetectivity of 3.09×10^{10} Jones.

Introduction

Organic-Inorganic halide perovskites have been in the limelight since its inception as the active material for the solar cells in 2009.[1] The large exciton diffusion lengths, low bandgaps and ease of processability make them the potential candidates for solar cells with superior power conversion efficiencies approaching the Shockley-Queisser limit.[2] Apart from the solar cells, perovskites are also used in light emitting diodes, [3, 4] photo-detectors, [5] nanoscale lasers [6] and nonlinear optical devices.[7] There are quite a few papers published on these interesting materials mainly as absorbers in the solar cells [1, 8-11] with certified efficiencies more than 25%. [12-15]

Recently, the Ruddlesden–Popper (RP) perovskite, a two-dimensional (2D) analogue of organometallic methylammonium lead halide perovskite is emerged as a moisture resistant and stable material to address the instability issues of perovskite solar cells.[16-18] The 2D RP perovskites are composed of 1-4 2D semiconducting inorganic layers separated by insulating organic layers, unlike the 3D perovskites in which a large number of inorganic layers are closely packed between the organic layers. The inorganic layers in the 2D RP perovskites act as quantum wells and the organic layers form the potential barrier to separate them. The optoelectronic properties of these materials can be fine-tuned by adjusting the number of semiconducting layers and the distance between them.[19] Large Bohr radii and highly stable excitons with very high binding energies are generated because of the nanometer-scale confinement of charge carriers in these semiconductors.[17] It has also been revealed that the very high excitonic stability arises from the modulated dielectric properties due to the organic material in these compounds rather than the quantum confinement effect alone.[17] Lately, Stoumpos et al. [17] reported a detailed synthesis, crystal structure analysis and characterization of linear optical properties of these interesting materials and demonstrated its potential use in highly stable solar cells. Stronger confinement effects can be expected if the dimensionality of these stable perovskites can be reduced to nanosizes which could enhance and extend the use of these materials in diverse applications. However, to the best of our knowledge, there are no reports on the synthesis of nanoplatelets of these homologous 2D series of RP perovskites of the kind $(CH_3(CH_2)_3NH_3)_2(CH_3NH_3)_{n-1}Pb_nI_{3n+1}$ (where n can be 1, 2, 3, or 4) by a reflux pre-treatment mediated sonication method. The 2D perovskites with n = 2 to 4 are a class of naturally forming superlattice semiconductors that shows unique optoelectronic properties different from n = 1 with varying thicknesses.[17]

In this work, we implemented a reflux pre-treatment mediated ultrasonication method for the first time to synthesize stable 2D RP nanoplatelets of width ~ 5 nm and length ~ 40 nm. The synthesized bulk 2D RP perovskite crystals and nanoplatelets are of the kind $(BA)_2(MA)_{n-1}Pb_nI_{3n+1}$ where n=2. The 2D RP nanoplatelets were characterized by UV-visible absorption spectroscopy, photoluminescence spectroscopy (PL), X-ray diffraction (XRD) analysis, transmission electron microscope (TEM) imaging, X-ray photoelectron spectroscopy (XPS) and Kelvin probe force microscope (KPFM) imaging. KPFM provides the surface potential of the sample with respect to the work function of the uncontacted tip. Any significant change in the surface potential/work function can be due to confinement effects as a result of the smaller size of the nanoplatelets. The photoresponse of the nanoplatelets was studied by fabricating a photodetector and was found to achieve remarkably fast response time which is comparable to the other perovskites-based photodetectors reported in the literature with the same device configuration.[20-22]

Results and discussion

In the present work, we have successfully synthesized the 2D RP nanoplatelets with formula $(CH_3(CH_2)_3NH_3)_2(CH_3NH_3)Pb_2I_7$ (n=2) from the bulk 2D RP crystals synthesized according to a reported literature[17]. The nanoplatelets of 2D RP perovskite were prepared from the parent cherry-red crystals by a reflux pre-treatment-mediated ultrasonication method. The synthesis of bulk 2D RP crystals and nanoplatelets are schematically shown in Fig. 1a. The SEM image of the bulk 2D RP crystals is given in Fig. S1 (ESI) from which the size of crystals is several micrometers. We have examined the elemental composition of the as-synthesized bulk 2D RP crystals by EDX mapping (Fig. S2, ESI) and confirmed the synthesis of lead iodide-based organic–inorganic hybrid perovskite. These bulk 2D RP crystals are further used to synthesize 2D RP nanoplatelets. Initially, the bulk 2D RP crystals are taken in a non-solvent toluene, was refluxed for 30 minutes under vigorous stirring. The resultant dispersion in toluene was ultrasonicated in a water bath for 5 minutes followed by filtration using a 0.22 μm PTFE membrane syringe filter to get the nanoplatelets. The samples were also prepared by just bathsonicating and probe-sonicating the dispersions of the 2D RP crystals in toluene. Both the methods gave 2D RP quantum dots (Fig. S3, ESI). The detailed study and results will be communicated in another article. Any further increase in reflux time or sonication time had no influence in further reduction in the platelet size, but seemed to degrade the sample as evident from the colour change. The reflux-mediated ultrasonication method for the synthesis of 2D RP nanoplatelets can thus be considered as a universal method for synthesizing 2D RP nanoplatelets and may be extended to other types of perovskites too. The optical and electrical properties of the 2D RP perovskite $(CH_3(CH_2)_3NH_3)_2(CH_3NH_3)_{n-1}Pb_nI_{3n+1}$) varies significantly with the number of layers denoted by the order ‘n’.

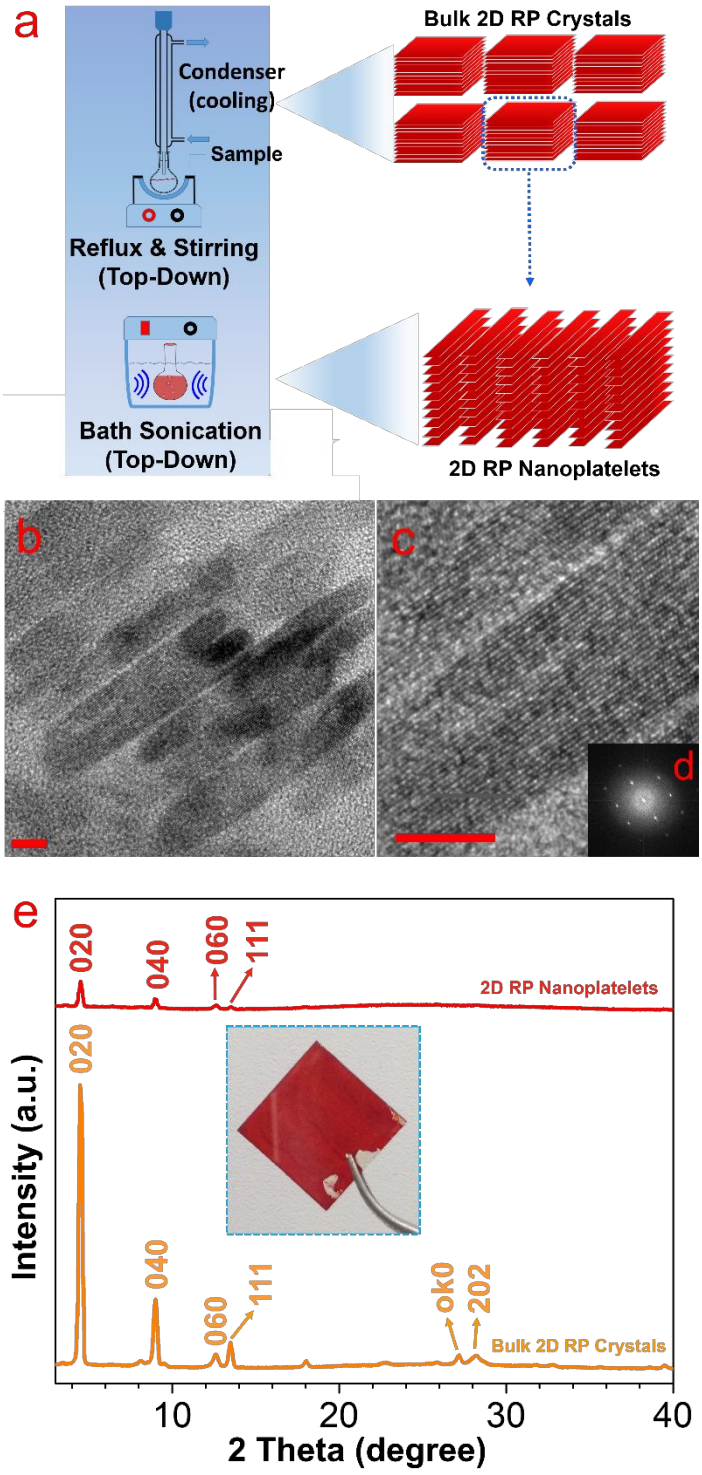

Fig. 1. (a) Schematic depicting the synthesis of bulk 2D RP crystals and nanoplatelets in which 2D RP layers in toluene kept under vigorous stirring while refluxing splits the layers into smaller fragments and forms as 2D RP nanoplatelets by bath sonication; (b, c) HRTEM images of 2D RP nanoplatelets (scale bar: 5 nm) and the corresponding FFT image (d); (d) XRD spectra of bulk 2D RP film and nanoplatelets (inset: digital photograph of a film made on glass slide).

The high-resolution transmission electron microscope (HRTEM) images of the 2D RP nanoplatelets are shown in Fig. 1b and Fig. 1c. The FFT image (Fig. 1d) processed from Fig. 1c shows the crystalline nature of the nanoplatelets. The 2D RP nanoplatelets with an average width of ~ 4.75 nm and length of ~ 45 nm can be clearly visible in the HRTEM image (Fig. S4, ESI). The fast Fourier transform (FFT) of the TEM image is shown in the inset of Fig. 1c. The profile analysis (Fig. S4, ESI) of HRTEM image (Fig. 1c) shows the (222) plane corresponding to the d-value 3.13nm. [17] The XRD spectra of 2D RP film and nanoplatelets are shown in Fig. 1d. The 2D RP film can be considered equivalent to the 2D RP crystals as it form perovskite crystals of several micrometers when spincoated on heated glass substrates.[17,18] For the bulk 2D RP film, the XRD peaks positioned at 4.51°, 9.02°, 12.65°, 13.49°, 17.97°, 27.13°, 28.19°, and 28.84° corresponds to (020), (040), (060), (111), (080), (0k0), (202), and (222) reflections respectively. These reflections are found well matched with the $(BA)_2(MA)Pb_2I_7$ film in the literature.[17, 18] Thus the synthesis of $(BA)_2(MA)_{n-1}Pb_nI_{3n+1}$ where n = 2 material is confirmed. In the case of reflections of nanoplatelets prepared by the reflux method shows broader peaks at the same positions with lower intensities with respect to that of the bulk 2D RP film due to the reduction in the particle size. It was also evident from the XRD since we did not find any peaks corresponding to other structures/materials. A digital photograph of the film coated on a glass substrate using 2D RP nanoplatelets is shown in the inset of Fig. 1d. The UV-visible absorption spectrum of bulk 2D RP film has a wide absorption that spans from the ultraviolet to the red wavelengths is shown in the inset of Fig. 2a.[17] The UV-visible spectrum shown in Fig. 2a corresponds to the 2D RP nanoplatelets. A substantial blue shift in the absorption peaks with excitonic peaks at ~ 304 nm and a smaller absorption peak at ~ 496 nm confirms the size reduction.[23] Apart from the primary absorption edge, we have observed a second peak, which is usually very prominent in the case of n=1 and progressively decreases as the number of inorganic slabs increases.[18] The second absorption peak is attributed to the long-lived excitonic state trapped in the strong electrostatic field created by the localized BA ions (positively charged) around the $MA_{n-1}Pb_nI_{3n+1}$ (negatively charged) layers.[18, 24] The UV-visible absorption spectrum of the 2D RP nanoplatelets (Fig. S5, ESI) stored in a glass in ambient atmosphere shows no significant shift in their peak positions even after 60 days and hence it can be said that the as-synthesized 2D RP nanoplatelets exhibits excellent stability in air. It is to be noted here that the stability is the bottleneck of using perovskites for commercial applications. But the present study opens-up a new perovskite material with high stability. Unlike the 2D RP film which shows photoluminescence (PL) emission at about 612 nm (shown in the inset of Fig. 2b, excitation wavelength – 350nm), the 2D RP nanoplatelets show very intense PL with a blue shift as shown in Fig. 2b. It shows an enhanced and broader emission peak at 348 nm (excitation wavelength - 304nm) due to the lateral size confinement.[23] The absorption at UV frequencies is attractive for applications such as UV detectors, UV-based sensors, etc.

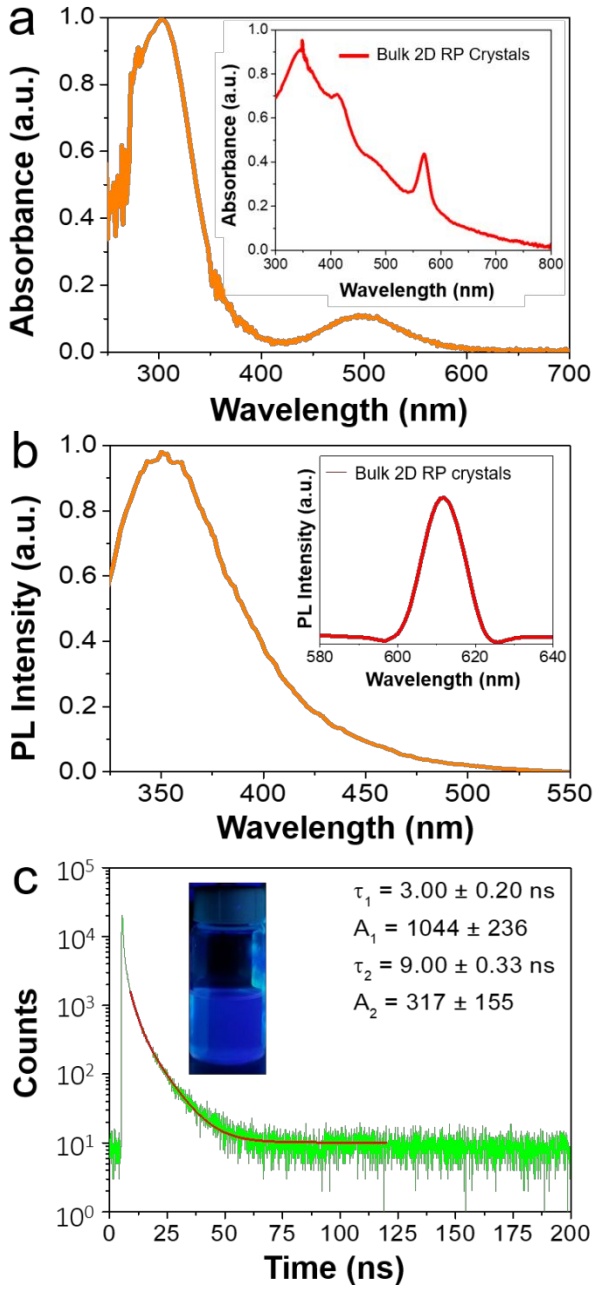

Fig. 2. (a) UV-Vis absorption spectrum of 2D RD nanoplatelets (inset figure for bulk 2D RP crystals); (b) PL spectrum of the 2D RP nanoplatelets (inset figure for bulk 2D RP crystals); (c) Fluorescence lifetime decay (green) and fitting curve (red) for excitation at 373 nm and emission at > 400 nm for the 2D RP nanoplatelets (inset shows the digital image of the 2D RP nanoplatelets under UV illumination).

Excited state dynamics of the 2D RP nanoplatelets were studied with the time-correlated single photon counting technique (TCSPC) by determining the lifetime of the excited state of the 2D RP nanoplatelets. The fluorescence lifetime data was obtained for the 2D RP nanoplatelets. A decay curve for the 2D RP nanoplatelets is shown in Fig. 2c which can be fitted to a biexponential decay function with a τ_1 of 3.00 ± 0.20 ns and τ_2 of 9.00 ± 0.33 ns for the refluxed

2D RP nanoplatelets. We found that the excited state lifetimes for the 2D RP nanoplatelets fall within the nanosecond time scale. Reported fluorescence decay in perovskite materials shows biexponential behaviour with lifetime values ranging from the sub-nanosecond time scale to a few nanoseconds for the dominant shorter component, while the longer component is reported to be in the nanosecond range.[1, 2, 4] The 2D RP nanoplatelets sample examined in this study were also found to exhibit a biexponential decay, and display lifetime values in agreement with those found in the recent literature for hybrid 2D perovskite structures.[3, 5] The high photoluminescence intensity in addition to the broadened steady-state PL spectrum and short PL lifetimes indicates the excited state dynamics are being influenced by both quantum and dielectric confinement in the sample.[25-27] Increased confinement effects in the 2D RP nanoplatelets increases the probability that the photoluminescence lifetime decay is influenced by lattice vibrations, which would indicate the presence of exciton-phonon coupling.[28] Recently, *Stoumpos, et. al.* investigated the band structure of $(CH_3(CH_2)_3NH_3)_2(CH_3NH_3)_{n-1}Pb_nI_{3n+1}$ (n = 1, 2, 3, 4, ∞) and found that the valance band was almost entirely comprised of I 5p and Pb 6s states while the conduction band was composed mostly of Pb 6p states. The valance and conduction bands were revealed to constitute a distinct direct band gap, which decreases in energy with increasing number of perovskite layers.[17] In addition, because the 2D RP semiconducting network is disconnected in one direction (due to the quantum well structure) it restricts movement of excitons in one direction, along the perovskite material confined by organic spacer molecules.[17] Instances of exciton-phonon coupling due to quantum and dielectric confinement are further supported by claims of high exciton binding energies reported for both $MAPbI_3$ individually[29] and 2D RP homologues.[30] The high exciton binding energies should produce a narrow photoluminescence spectrum with longer average lifetimes though we observe a broad photoluminescence spectrum (figure 2b) with shorter average lifetimes for 2D RP nanoplatelets. This provides further evidence to emission interference by lattice vibrations, which may be creating self-trapped exciton states recognized in 2D materials.[28] These short-lived excited states also allow for a higher excitation rate that results in the overall high photoluminescence intensity seen in the sample. Inset of Fig. 2c shows the digital image of the 2D RP nanoplatelets under UV illumination.

KPFM is a versatile and powerful tool to analyse the work function of the materials with nanometer resolution by measuring the contact potential difference (CPD) between the tip of the AFM cantilever and the sample. It gives precise information on the changes due to confinement effects or surface modification.[31] When electrically connected AFM tip of dissimilar energy level (with respect to sample) approaches a sample, the Fermi levels of both materials get aligned due to the electron flow from one material to the other. The sample surface can be negative or positive due to addition or removal of electrons, respectively, and Coulomb's law gives the electrostatic forces. This electrostatic force can be nullified by providing an external bias by injecting electrons when the applied bias is equal to the difference in Fermi levels.[31] A schematic of the KPFM and the respective band diagrams explaining this process are illustrated in Fig. 3a-c. Here, we analyzed the topography and CPD on the surface of a thin film prepared with the bulk 2D RP crystals and the 2D RP nanoplatelets prepared by the reflux method (Fig. 3d-g). The KPFM chamber was maintained under nitrogen atmosphere during the experiment and the distance between the sample and the probe was maintained to be same for both the samples under study.

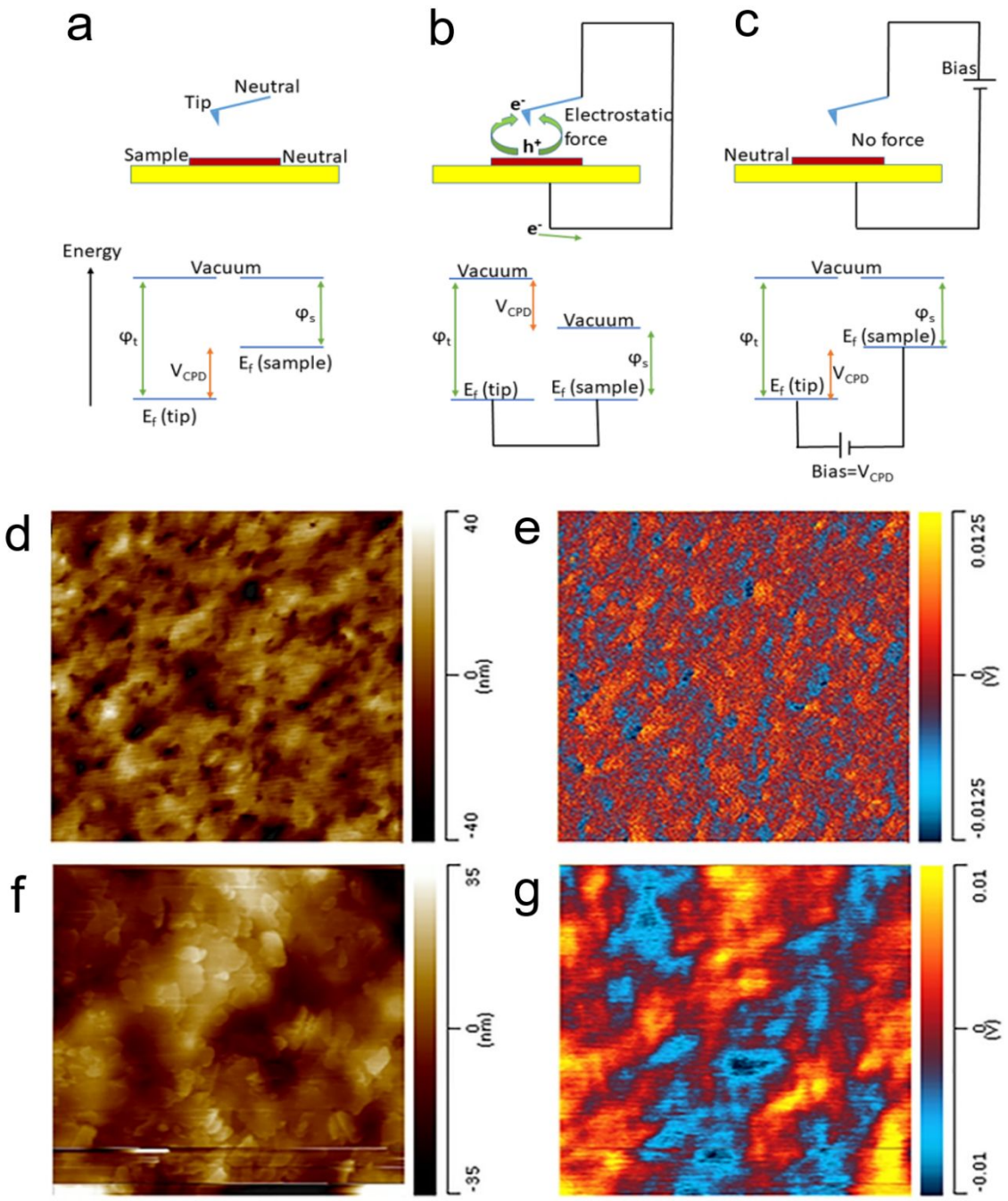

Fig. 3. (a-c) Schematic of KPFM and respective band diagrams, flattened topography (d and f) and KPFM (e and g) images of bulk 2D RP crystals and 2D RP nanoplatelets prepared by reflux method respectively (scale bar: 5 µm X 5 µm).

The work function of the platinum-iridium tip was calibrated using a freshly cleaved HOPG surface and found to be 4.82 eV. The 2D RP perovskite film returned a CPD of 6.42×10^{-2} V and the nanoplatelets gave 0.136 V as shown in Fig. 3e and Fig. 3g, respectively. The work function of the bulk 2D RP crystals and nanoplatelets determined from the CPD values are ~ 4.88 eV and ~ 4.96 eV, respectively. The work function of the bulk 2D RP crystals agrees well with the

reported value of 4.88 eV obtained from the ultraviolet-photoelectron spectroscopy experiments.[18] A significant difference of 0.08 eV can be observed in the case of 2D RP nanoplatelets compared with that of the bulk 2D RP crystals. This change in the work function can be attributed to the difference in the surface energy as a result of the modified quantum confinement effects in the nanoplatelets when the bulk 2D RP crystals are broken into smaller dimensions during probe sonication. The topographical image, shown in Fig. 3f, confirms the nanoplatelets geometry of the sample prepared using the reflux method. The thickness of nanoplatelets were analysed from the AFM topography image (Fig. S6, ESI) and is found to be about 5nm which agrees well with that estimated from the HRTEM image.

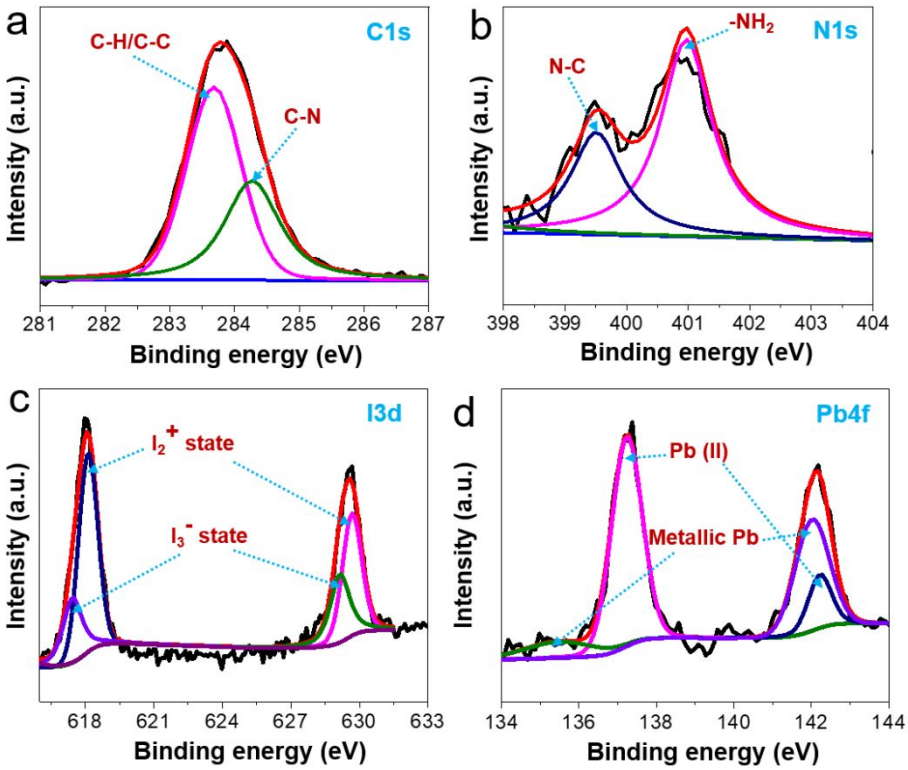

Fig. 4. XPS core-level C1s (a), N 1s (b), I 3d doublets (c), and Pb 4f doublets (d) spectra of bulk 2D RP crystals.

XPS was used to examine the chemical states of the as-synthesized bulk 2D RP crystals and nanoplatelets. The XPS data were fitted with Gaussian–Lorentzian functions with a Shirley type background. The high-resolution XPS core-level C1s, N1s, I3d doublets ($3d_{5/2}$ and $3d_{3/2}$), Pb4f doublets ($4f_{7/2}$ and $4f_{5/2}$) spectra of the bulk 2D RP crystals and nanoplatelets are depicted in Fig. 4 and Fig. 5, respectively. The de-convoluted C1s spectra of the bulk 2D RP crystals exhibit peak at 283.68 eV which corresponds to aliphatic hydrocarbon (C-H or C-C) and one at 284.27 eV corresponds to carbon atoms bonded with single nitrogen atoms (C-N) (Fig. 4a). However for nanoplatelets, these peaks are shifted to 283.84 eV and 285.12 eV (Fig. 5a), respectively. The N1s spectra of the bulk 2D RP crystals exhibited two major peaks located at 399.51 eV and 400.97 eV, which are assigned to the single-bonded nitrogen atom with the carbon atom (N-C), and the amide ions ($-NH_2$) (Fig. 4b) whereas in the case of nanoplatelets, these peaks are shifted

to 400.98 eV and 401.49 eV (Fig. 5b), respectively.[32] The core-level XPS I3d doublets spectra of bulk 2D RP crystals appeared at 629.67 eV and 618.13 eV (which correspond to the I_2^+ charge state) and 629.14 eV and 617.44 eV (which correspond to the I_3^- charge state (Fig. 4c).[33] However, for 2D RP nanoplatelets, these peaks are shifted to 630.06 eV and 618.49 eV which correspond to the I_2^+ charge state and 629.55 eV and 618.01 eV correspond to the I_3^- charge state (Fig. 5c), respectively.[33] The Pb4f doublets of the bulk 2D RP crystals appeared at 137.23 eV and 142.22 eV correspond to Pb (II); 135.48 eV and 142.01 eV correspond to metallic Pb (Fig. 4d) but for 2D RP nanoplatelets, these peaks are shifted to 137.38 eV and 142.28 eV correspond to Pb (II) and 135.95 eV and 142.15 eV correspond to metallic Pb (Fig. 5d), respectively.[33] In all spectra, a shift towards higher binding energy is observed for the 2D RP nanoplatelets compared to the bulk 2D RP crystals. To interpret the positive binding energy shift, the final state of the photoemission process must be considered. The emitted photoelectrons from the 2D nanoplatelets create a net positive charge on the nanoplatelets. As a result, the Coulomb interaction leads to reduction in the kinetic energy of the photoelectron which in turn appears as a positive shift in the binding energy in the spectrum. [34] Hence in this case, the positive shift in the XPS spectra can be attributed to the quantum-size effect. As the dimension of the 2D RP perovskite decreases, the electronic energy states are localized which creates a quantum confinement effect, therefore their binding energy increases with respect to the bulk 2D RP crystals. The bulk 2D RP crystals of the type n=2 shows a confinement effect resulting from the number of semiconducting layers in the material separated by organic spacers. In general, the bulk 2D RP crystals show confinement as they are quantum well structures. However, in the case of 2D RP nanoplatelets, further confinement can happen due to the lateral size confinement. This lateral size confinement of 2D RP nanoplatelets is due to the average width of ~ 5 nm and length of ~ 40 nm as can be seen from the TEM image discussed previously (Fig. 1b). In the case of XRD data of nanoplatelets, a broadening in the peaks is observed due to the reduction in the particle size. This is supported by a difference in the binding energies of the nanoplatelets as observed from the XPS analysis compared to the bulk 2D RP crystals. Hence, confinement effect in the nanoplatelets is evident from the morphological, optical and structural characterizations.

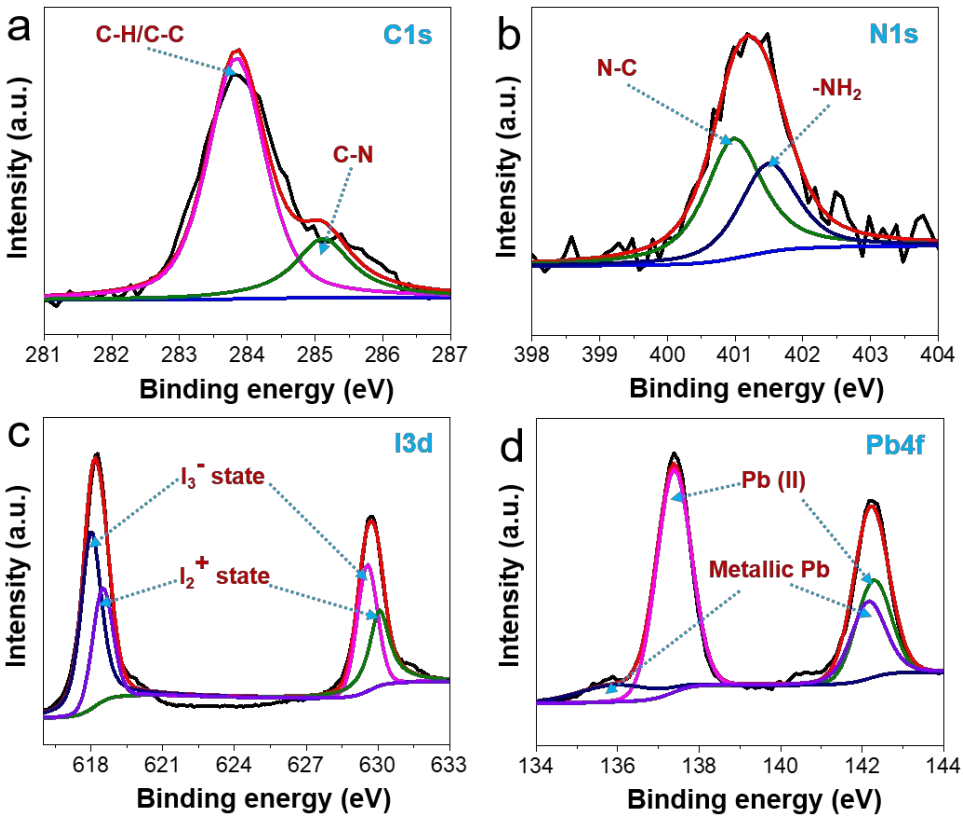

Fig. 5. XPS core-level C1s (a), N 1s (b), I 3d doublets (c), and Pb 4f doublets (d) spectra of 2D RP nanoplatelets.

Stronger quantum confinement in 2D RP nanoplatelets make them very attractive compared with the 3D perovskites for wavelength tunability and for optical signal detectivity. To test this hypothesis, we fabricated a photodetector using as-synthesized 2D RP nanoplatelets. The 2D RP nanoplatelets were drop casted on the pre-fabricated Cr/Au electrodes on glass substrates. The schematic device architecture is shown in the inset of Fig. 6a. The current-voltage (I-V) characteristics of 2D perovskite nanoplatelet device is presented in the Fig. 6a under dark and illumination of monochromatic light of wavelength 550 nm with an intensity of 33 $\mu W/cm^2$. When light is incident on the 2D RP nanoplatelets, it absorbs the photon energy thus creating excitons, which are dissociated at the interface and are transferred to the respective electrodes by hopping or tunnelling mechanism through the conductive channels within the nanoplatelets.[35] The 2D RP nanoplatelet based photodetector shows a maximum photoresponsivity (R in A/W) of 4.5×10^{-3} A/W at 10 V applied bias. It also shows a detectivity (D*) of 3.09×10^{10} Jones, which is the ability of a photodetector to detect weak light signals. The broadband photoresponse of 2D nanoplatelets under periodic illumination with on and off intervals of 15s at four different wavelengths, 400 nm, 550 nm, and 580 nm are shown in Fig. 6b. It displays a fast photoresponse to optical signal when biased at 10 V. It has also been observed that the photocurrent density improves with increasing incident photon power. The spectral response of the 2D perovskite nanoplatelet photodetector investigated over the range of 400 to 580 nm for two different applied biases 5 V and 10 V is shown in Fig. 6c. Although, the UV-visible spectrum of 2D nanoplatelets

show strong absorption peak at 304 nm, but due to limitation of our experimental setup, we are unable to measure photoresponse in this wavelength.

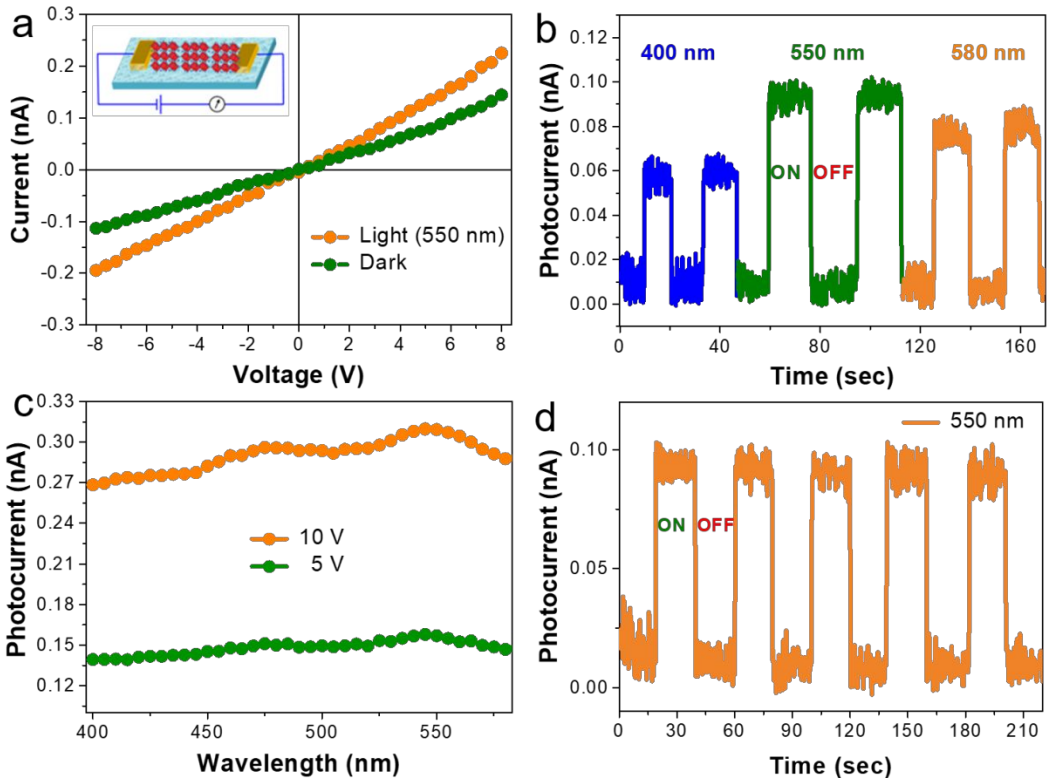

Fig. 6. (a) Current-voltage characteristics of 2D RP nanoplatelets under dark and illumination at 550 nm (inset: schematic of the device structure of the fabricated photodetector); (b) Photoresponse of 2D nanoplatelets under periodic illumination with an on/off interval of 15 s for four different wavelengths 400, 550, and 580 nm; (c) Spectral photocurrent response of 2D nanoplatelets under different wavelengths with two different bias voltages; (d) Transient photoresponse with 550 nm wavelength light illumination under on/off conditions.

The photocurrent response of the device increases with the applied bias voltage. This kind of broadband photodetection has a promising potential for various optoelectronics applications. The transient photoresponse of 2D nanopletelets under periodic illumination with on/off intervals of 20 s and the reliability investigated under 550 nm monochromatic light is shown in Fig. 6d. We found that dynamic photoresponse of this photodetector is very stable and reproducible. We also observed a quick rise in photocurrent as soon as the light is turned on and then drops to initial values as the light is turned off, which indicates that the device can act as a light activated switch. As 2D nanoplatelets are rectangular in shape with ~40 nm length, they can create conducting network which act as a channel for better charge transport between the electrodes as compared to only QDs network. When light is incident on the 2D RP nanoplatelets, it absorbs the photon energy thus creating excitons, which are dissociated at edge states in layered 2D nanoplatelets[36] and also in the interface between the nanoplatelets and metal contact and hence are transferred to the respective electrodes by hopping or tunnelling mechanism. Although, it is

found that the response time for the 2D perovskite photodetector is very fast (<100 ms), we were unable to measure it due to instrumental limitation.

Conclusions

We have presented a new method of preparing highly stable 2D RP nanoplatelets via reflux-mediated ultrasonication with a high stability under ambient atmosphere. A considerable change in the surface potential of the nanoplatelets compared with the bulk 2D RP crystals measured using KPFM and a peak shift towards higher binding energy in the core level XPS spectra for the nanoplatelets compared to that of the bulk 2D RP film is observed. This demonstrates that there is further quantum confinement when made into nanoplatelets compared to the bulk 2D RP film. The 2D RP nanoplatelets showed intense photoluminescence emission in the ultraviolet region with very short lifetimes. A photodetector fabricated with pristine nanoplatelets exhibited a high photodetectivity of 3.09×10^{10} Jones. The high PL emission and good photodetection characteristics exhibited by the 2D RP nanoplatelets open the door for these quantum confined perovskite nanostructures to be used for futuristic applications like photonics, phototransistors, and optoelectronic sensors.

Experimental methods

Materials

Lead oxide (PbO) (99.999%), hydroiodic acid (HI) (57 wt. % in H_2O), hypophosphorous acid (H_3PO_2) (50 wt. % in H_2O)., toluene (99.8%), and n-butylamine (99.5%) were purchased from Sigma-Aldrich, USA. Methylammonium iodide (>99.5%) was purchased from Luminescence Technology Corp., Taiwan.

Synthesis of Bulk 2D RP perovskite crystals (n=2)

The bulk 2D RP crystals with n = 2 were synthesized according to the procedure reported in the literature.[16-18] Briefly, PbO was dissolved in a mixture of 57% w/w aqueous HI and 50% aqueous hypophosphorous acid (H_3PO_2) by heating under magnetic stirring for 5 min. Methylammonium iodide (MAI) was added to the resultant hot solution under constant stirring and a black precipitate appears which re-dissolves to provide a bright yellow solution. N-butylamine (248 μL) was mixed with 5 mL HI solution separately in a vial kept in an ice bath. The n-butylamine solution was then added drop-wise to the hot PbO solution in the acid mixture. The bright yellow solution was then allowed to cool to room temperature after 5 min of constant stirring and heating. The 2D RP perovskite in the form of cherry-red crystals were obtained by suction filtration and drying under reduced pressure. The 2D RP films of this parent material were spincoated on heated glass-slides at 2000 rpm for 30s.

Characterizations

The topography of 2D RP nanoplatelets was characterized by TEM (FEI Tecnai F30 TEM) and AFM/IR System (Anasys Instruments NanoIR 2). The structure of 2D RP nanoplatelets was determined using XRD analysis (PANalytical Empyrean with 1.8 KW Copper X-ray Tube) and UV-Vis absorption spectroscopy (UV-Vis Spectrophotometer – Agilent Cary 300). The photoluminescence spectra of the samples were recorded using fluorescence spectroscopy (Fluorescence Spectrometer - Horiba Nanolog FL3-11). The 2D RP bulk film and nanoplatelets cast on optically transparent glass-slides were used for optical characterizations. The chemical

bonding states of the materials were examined in detail by XPS (Physical Electronics 5400 ESCA). The high-resolution XPS spectra corresponding to C1s, N1s, I3d doublets ($3d_{5/2}$ and $3d_{3/2}$), and Pb4f doublets ($4f_{7/2}$ and $4f_{5/2}$) were analysed using XPS Peak version 4.1 program. Kelvin probe AFM measurements (Anasys Instruments NanoIR2) were carried out to find out the surface potential of the 2D RP nanoplatelets. The surface potential analyses were performed in the unprocessed topography image from the AFM.

Time correlated single photon counting (TCSPC)

Time correlated single photon counting (TCSPC) curves were collected while exciting the samples with a PicoQuant LDH-P-C-375 pulsed laser driven by a PDL 800D controller. The repetition rate was set at 5 MHz. Laser intensity was adjusted to excitation powers under 10^{-6} W/cm^2 to stay below the photon emission rate limit of 5% for appropriate TCSPC data collection to eliminate pile up effects. Photons were collected on a single photon counting detector (Picoquant, sMicro Photon Devices, PDM series) connected to a PicoHarp 300 TCSPC module that detects the photon arrival time. The laser excitation was filtered with a 375 nm interference filter while the emission was filtered by a 400nm long pass emission filter. TCSPC decay curves were fitted with FluoFit software (FluoFit Pro 2009, 4.4.0.1, PicoQuant). Since TCSPC decays were collected locally on 2D perovskite nanostructures using a custom built microscope[6] an IRF is not obtained, and decay curve fitting was accomplished via a tail fitting process. In the tail fitting process, the rise of the exponential decay curve and the region where the IRF is expected are ignored to remove the need for deconvolution between decay and IRF.

Fabrication of photodetector

The pattern Cr/Au (5 nm/50 nm) electrodes were fabricated on glass substrate by thermal evaporation through a designed metal mask to form 80 μm channel length. Toluene solution of as-synthesised 2D RP nanoplatelets are drop-casted on pre-fabricated Cr/Au electrode and dried at room temperature. The current-voltage (*I-V*) characteristics were measured using Keithley 2400 source meter under the illumination from a halogen lamp fitted with Newport monochromator. The spectral photocurrent response was measured by a source meter and the light intensity was measured using Newport power meter through calibrated Si photodiode. All photodetector measurements were conducted at ambient room temperature conditions.

Conflicts of interest

There are no conflicts to declare.

Acknowledgements

JT acknowledges National Science Foundation (CAREER: ECCS-1351757) for the financial support. EB acknowledges NASA Space Technology Research Fellowship Program for XPS analysis. SJV thanks the University Grants Commission, Government of India for supporting visiting scholar program (Raman PDF, F.No.5-166/2016(IC)) in the USA. JC thanks the P3 Pre-Eminent Post-Doctoral Research Fellowship awarded by the University of Central Florida, Florida, USA.

Author contributions

JC, SJV and MZA prepared the bulk 2D RP crystals and nanoplatelets with feedback from JT. SJV and JC carried out the optical and structural characterization of the samples. AT and AG

performed the PL lifetime measurements. BP, JL and JC designed, fabricated and characterized the photodetector with feedback from JT. JT directed the overall research of this project. All the authors contributed to the discussion of the paper and approved the manuscript.

Permanent address of SJV: Department of Physics, Sanatana Dharma College, Alappuzha, Kerala, India – 688003. Permanent address of BP: Centre of Excellence in Green and Efficient Energy Technology, Department of Energy Engineering, Central University of Jharkhand, Brambe, Ranchi, Jharkhand, India-835205.

JC and SJV contributed equally to this work.

Notes and references

1. A. Kojima, K. Teshima, Y. Shirai and T. Miyasaka, *Journal of the American Chemical Society*, 2009, **131**, 6050-6051.
2. W. E. I. Sha, X. G. Ren, L. Z. Chen and W. C. H. Choy, *Applied Physics Letters*, 2015, **106**.
3. Y. Ling, Z. Yuan, Y. Tian, X. Wang, J. C. Wang, Y. Xin, K. Hanson, B. Ma and H. Gao, *Advanced Materials*, 2016, **28**, 305-311.
4. Z.-K. Tan, R. S. Moghaddam, M. L. Lai, P. Docampo, R. Higler, F. Deschler, M. Price, A. Sadhanala, L. M. Pazos and D. Credgington, *Nature nanotechnology*, 2014, **9**, 687-692.
5. X. Hu, X. Zhang, L. Liang, J. Bao, S. Li, W. Yang and Y. Xie, *Advanced Functional Materials*, 2014, **24**, 7373-7380.
6. H. Yu, K. Ren, Q. Wu, J. Wang, J. Lin, Z. Wang, J. Xu, R. F. Oulton, S. Qu and P. Jin, *Nanoscale*, 2016, **8**, 19536-19540.
7. R. Zhang, J. Fan, X. Zhang, H. Yu, H. Zhang, Y. Mai, T. Xu, J. Wang and H. J. Snaith, *ACS Photonics*, 2016, **3**, 371-377.
8. L.-C. Chen, Z.-L. Tseng and C.-C. Wang, *Materials Science in Semiconductor Processing*, 2016, **56**, 179-182.
9. D. P. McMeekin, G. Sadoughi, W. Rehman, G. E. Eperon, M. Saliba, M. T. Hörantner, A. Haghighirad, N. Sakai, L. Korte and B. Rech, *Science*, 2016, **351**, 151-155.
10. C. Li, J. Sleppy, N. Dhasmana, M. Soliman, L. Tetard and J. Thomas, *Journal of Materials Chemistry A*, 2016, **4**, 11648-11655.
11. C. Li, M. M. Islam, J. Moore, J. Sleppy, C. Morrison, K. Konstantinov, S. X. Dou, C. Renduchintala and J. Thomas, *Nature communications*, 2016, **7**, 13319.
12. R. Service, *Science (New York, NY)*, 2016, **354**, 1214.
13. J.-P. Correa-Baena, A. Abate, M. Saliba, W. Tress, T. J. Jacobsson, M. Grätzel and A. Hagfeldt, *Energy & Environmental Science*, 2017, **10**, 710-727.
14. K. E. Martin A. Green, Yoshihiro Hishikawa, Wilhelm Warta, Ewan D. Dunlop, Dean H. Levi, Anita W. Y. Ho-Baillie, *Progress in Photovoltaics: Research and Applications*, 2016, **25**, 3-13.
15. https://www.nrel.gov/pv/cell-efficiency.html..
16. H. Tsai, W. Nie, J.-C. Blancon, C. C. Stoumpos, R. Asadpour, B. Harutyunyan, A. J. Neukirch, R. Verduzco, J. J. Crochet and S. Tretiak, *Nature*, 2016, **536**, 312.
17. C. C. Stoumpos, D. H. Cao, D. J. Clark, J. Young, J. M. Rondinelli, J. I. Jang, J. T. Hupp and M. G. Kanatzidis, *Chemistry of Materials*, 2016, **28**, 2852-2867.

18. D. H. Cao, C. C. Stoumpos, O. K. Farha, J. T. Hupp and M. G. Kanatzidis, *Journal of the American Chemical Society*, 2015, **137**, 7843-7850.
19. J.-C. Blancon, H. Tsai, W. Nie, C. C. Stoumpos, L. Pedesseau, C. Katan, M. Kepenekian, C. M. M. Soe, K. Appavoo and M. Y. Sfeir, *Science*, 2017, eaal4211.
20. P. Li, B. Shivananju, Y. Zhang, S. Li and Q. Bao, *Journal of Physics D: Applied Physics*, 2017, **50**, 094002.
21. M. He, Y. Chen, H. Liu, J. Wang, X. Fang and Z. Liang, *Chemical Communications*, 2015, **51**, 9659-9661.
22. Y. Wang, Z. Xia, S. Du, F. Yuan, Z. Li, Z. Li, Q. Dai, H. Wang, S. Luo and S. Zhang, *Nanotechnology*, 2016, **27**, 175201.
23. H. Huang, L. Polavarapu, J. A. Sichert, A. S. Susha, A. S. Urban and A. L. Rogach, *NPG Asia Materials*, 2016, **8**, e328.
24. E. A. Muljarov, S. G. Tikhodeev, N. A. Gippius and T. Ishihara, *Phys Rev B*, 1995, **51**, 14370-14378.
25. X. X. Wu, M. T. Trinh, D. Niesner, H. M. Zhu, Z. Norman, J. S. Owen, O. Yaffe, B. J. Kudisch and X. Y. Zhu, *Journal of the American Chemical Society*, 2015, **137**, 2089-2096.
26. X. Hong, T. Ishihara and A. V. Nurmikko, *Phys Rev B*, 1992, **45**, 6961-6964.
27. M. D. Smith, L. Pedesseau, M. Kepenekian, I. C. Smith, C. Katan, J. Even and H. I. Karunadasa, *Chem Sci*, 2017, **8**, 1960-1968.
28. Y. Lekina and Z. X. Shen, *J Sci-Adv Mater Dev*, 2019, **4**, 189-200.
29. V. D'Innocenzo, G. Grancini, M. J. P. Alcocer, A. R. S. Kandada, S. D. Stranks, M. M. Lee, G. Lanzani, H. J. Snaith and A. Petrozza, *Nature Communications*, 2014, **5**.
30. O. Yaffe, A. Chernikov, Z. M. Norman, Y. Zhong, A. Velauthapillai, A. van der Zande, J. S. Owen and T. F. Heinz, *Phys Rev B*, 2015, **92**.
31. W. Melitz, J. Shen, A. C. Kummel and S. Lee, *Surface science reports*, 2011, **66**, 1-27.
32. T.-W. Ng, C.-Y. Chan, M.-F. Lo, Z. Q. Guan and C.-S. Lee, *Journal of Materials Chemistry A*, 2015, **3**, 9081-9085.
33. G. R. Kumar, A. D. Savariraj, S. N. Karthick, S. Selvam, B. Balamuralitharan, H. J. Kim, K. K. Viswanathan, M. Vijaykumar and K. Prabakar, *Physical Chemistry Chemical Physics*, 2016, **18**, 7284-7292.
34. M. Büttner and P. Oelhafen, *Surface science*, 2006, **600**, 1170-1177.
35. K. E. Knowles, M. D. Peterson, M. R. McPhail and E. A. Weiss, *The Journal of Physical Chemistry C*, 2013, **117**, 10229-10243.
36. J. C. Blancon, H. Tsai, W. Nie, C. C. Stoumpos, L. Pedesseau, C. Katan, M. Kepenekian, C. M. M. Soe, K. Appavoo, M. Y. Sfeir, S. Tretiak, P. M. Ajayan, M. G. Kanatzidis, J. Even, J. J. Crochet and A. D. Mohite, *Science*, 2017, **355**, 1288-1291.